The Primordial Inflation Explorer (PIXIE)

Alan Kogut[a], David T. Chuss, Jessie Dotson[b], Eli Dwek[a], Dale J. Fixsen[a], Mark Halpern[c], Gary F. Hinshaw[c], Stephan Meyer[d], S. Harvey Moseley[a], Michael D. Seiffert[e], David N. Spergel[f], and Edward J. Wollack[a]

[a]Code 665, NASA Goddard Space Flight Center, Greenbelt, MD USA 20771;
[b]NASA Ames Research Center, Moffett Field, CA, USA 94035;
[c]Dept. of Physics & Astronomy, University of British Columbia, Vancouver, BC, Canada, V6T 1Z1;
[d]Dept of Astronomy & Astrophysics, University of Chicago, Chicago, IL, USA;
[e]Jet Propulsion Laboratory, MS 169-506, Pasadena, CA, USA 91109;
[f]Dept of Astrophysical Sciences, Princeton University, Princeton, NJ, USA 08544

ABSTRACT

The Primordial Inflation Explorer is an Explorer-class mission to measure the gravity-wave signature of primordial inflation through its distinctive imprint on the linear polarization of the cosmic microwave background. PIXIE uses an innovative optical design to achieve background-limited sensitivity in 400 spectral channels spanning 2.5 decades in frequency from 30 GHz to 6 THz (1 cm to 50 micron wavelength). Multi-moded non-imaging optics feed a polarizing Fourier Transform Spectrometer to produce a set of interference fringes, proportional to the difference spectrum between orthogonal linear polarizations from the two input beams. Multiple levels of symmetry and signal modulation combine to reduce the instrumental signature and confusion from unpolarized sources to negligible levels. PIXIE will map the full sky in Stokes I, Q, and U parameters with angular resolution 2.6 deg and sensitivity 0.2 μK per 1 deg square pixel. The principal science goal is the detection and characterization of linear polarization from an inflationary epoch in the early universe, with tensor-to-scalar ratio $r < 10^{-3}$ at 5 standard deviations. In addition, PIXIE will measure the absolute frequency spectrum to constrain physical processes ranging from inflation to the nature of the first stars to the physical conditions within the interstellar medium of the Galaxy. We describe the PIXIE instrument and mission architecture with an emphasis on the expected level of systematic error suppression.

Keywords: polarimeter, cosmic microwave background, Fourier transform spectrometer, bolometer

1. INTRODUCTION

The era of precision cosmology is upon us. With only 6 free parameters, the "concordance" model successfully fits data sampling the universe over some 15 orders of magnitude in age, from the abundance of light elements shortly after the Big Bang to surveys of the location and velocity of galaxies today. In this model, present-day structures form by gravitational infall and collapse seeded by a nearly scale-invariant power spectrum of adiabatic initial density perturbations. The geometry of the universe is nearly flat, dominated by a cosmological constant Λ currently accelerating the expansion of the universe. The matter content is dominated by cold dark matter observable only through its gravitational interactions; baryonic matter makes up only a few percent of the total density.[1–3]

Within this standard model, however, significant questions remain. The concordance ΛCDM model postulates that early in its history, the universe underwent a rapid period of superluminal expansion called inflation. Inflation provides an elegant explanation for the observed flatness and density fluctuations, but it relies on extrapolation of physics to energies greatly in excess of direct experimental data. Nor are the contents of the universe in this model well understood. Although high energy physics offers several attractive dark matter candidates,

Send correspondence to: Alan.J.Kogut@nasa.gov; telephone 1 301 286 0853

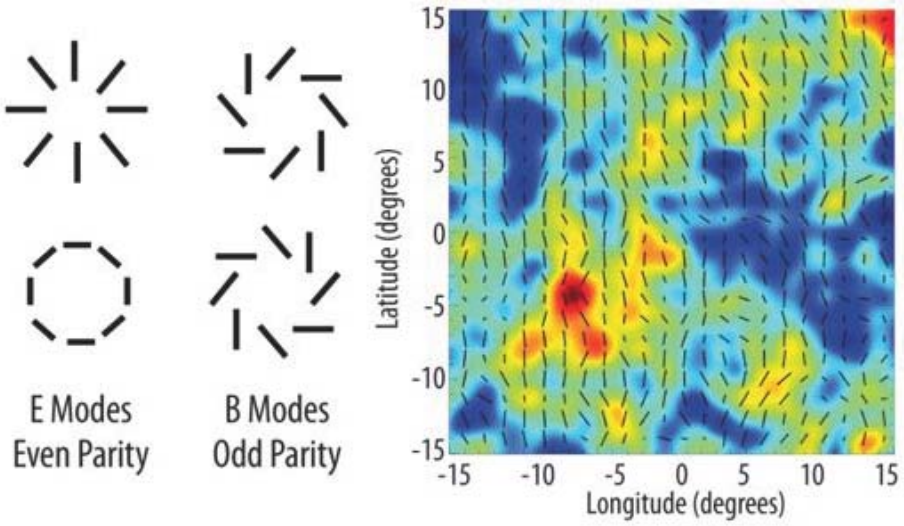

Figure 1. Simulated sky map showing CMB anisotropy (color) and polarization over a $30^\circ \times 30^\circ$ patch of sky. The polarization pattern can be decomposed into even-parity E-modes and odd-parity B-modes. Only gravitational waves can produce a B-mode signal in the CMB on large angular scales.

dark matter itself has never been directly observed. And despite considerable advances in hydrodynamical simulations, the processes by which the first stars form in a metal-free environment to reionize the universe remain unclear.

Measurements of the cosmic microwave background provide critical tests of the standard cosmological model. One such test is linear polarization. Gravitational waves created during an inflationary epoch interact with the CMB at much later epochs to create a distinctive signature in linear polarization. CMB polarization results from Thomson scattering of CMB photons by free electrons. Scattering of an isotropic radiation field produces no net polarization, but a quadrupole moment in the incident radiation yields a net polarized signal. There are only two possible sources for such a quadrupole: an intrinsic temperature anisotropy or the differential redshift caused by a propagating gravity wave. The two can be distinguished by their different spatial signatures (Figure 1). Temperature perturbations are scalar quantities; their polarization signal must therefore be curl-free. Gravitational waves, however, are tensor perturbations whose polarization includes both gradient and curl components. In analogy to electromagnetism, the scalar and curl components are often called "E" and "B" modes. Only gravitational waves induce a curl component: detection of a B-mode signal in the CMB polarization field is recognized as a "smoking gun" signature of inflation, testing physics at energies inaccessible through any other means.[4–11]

The amplitude of the gravitational wave signal depends on the inflationary potential

$$V^{1/4} = 1.06 \times 10^{16}\ \mathrm{GeV} \left(\frac{r}{0.01}\right)^{1/4} \tag{1}$$

where r is the power ratio of gravitational waves to density fluctuations. If inflation results from Grand Unified Theory physics (energy $\sim\ 10^{16}$ GeV), the B-mode amplitude should be in the range 1 to 100 nK. Signals at this amplitude could be detected by a dedicated polarimeter, providing a critical test of a central component of modern cosmology. Detection of a gravitational-wave component in the CMB polarization would have profound implications for both cosmology and high-energy physics. It would establish inflation as a physical reality, provide a direct, model-independent determination of the relevant energy scale, and test physics at energies a trillion times beyond those accessible to particle accelerators.

Distortions in the CMB blackbody spectrum provide a second powerful test for cosmology. Interactions between photons and charged particles at redshift $z > 2 \times 10^6$ rapidly establish thermal equilibrium, with the

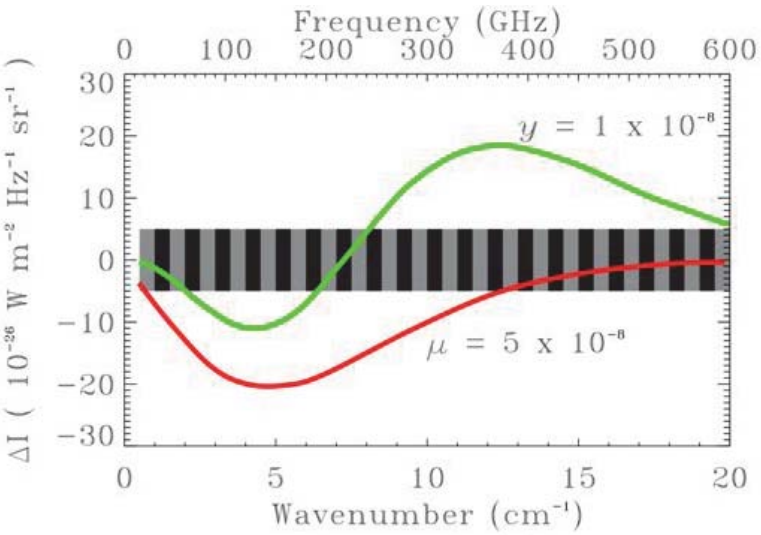

Figure 2. CMB spectral distortions. Solid curves show the difference between a blackbody spectrum and a chemical potential (red) or Compton spectrum (green) produced by energy releases in the early universe. Grey and black bars show the 1σ error bands for the proposed PIXIE mission. Known astrophysical processes should produce observable distortions, providing a new test of the standard cosmological model.

photon spectrum given by the familiar Planck formula

$$I(\nu, T) = \frac{2h\nu^3}{c^2} \frac{1}{\exp(h\nu/kT) - 1} \ , \tag{2}$$

where h is Planck's constant, k is Boltzmann's constant c is the speed lof light, ν is the frequency, and T is the phton temperature. Energy releases in at later redshift heat the electron gas, which then distorts the CMB spectrum as the CMB photons Compton scatter to higher energies. Once photon-creating processes become negligible at redshift $z \sim 2 \times 10^6$, the spectrum is unable to evolve to a (hotter) blackbody, locking in a spectral distortion. Such processes *must* exist within the standard cosmological model, distorting the CMB spectrum at observable levels. Figure 2 shows the distorted spectra. For early energy releases $2 \times 10^5 < z_r < 2 \times 10^6$, multiple scatterings create statistical equilibrium, leading to a distorted spectrum

$$I(\nu, T) = \frac{2h\nu^3}{c^2} \frac{1}{\exp(h\nu/kT - \mu) - 1} \tag{3}$$

with chemical potential

$$\mu = 1.4 \ \frac{\Delta E}{E} \tag{4}$$

proportional to the fractional energy release relative to the CMB.[12,13] Optically thin scattering at $z_r < 10^4$ generates a Compton distortion

$$\frac{\Delta I}{I} = y \frac{x e^x}{e^x - 1} \ \left[x \frac{e^x + 1}{e^x - 1} - 4 \right] \tag{5}$$

characterized by the parameter

$$y = \int \frac{k[T_e(z) - T(z)]}{m_e c^2} n_e(z) \sigma_T c \ dz, \tag{6}$$

where $x = h\nu/kT$, m_e, n_e, and T_e are the electron mass, number density, and temperature, and σ_T is the Thomson cross section,.[14] For intermediate redshifts $10^4 < z_r < 2 \times 10^5$ the spectrum is mixed.[15,16]

Upper limits $|\mu| < 9 \times 10^{-5}$ and $|y| < 15 \times 10^{-6}$ by the Cosmic Background Explorer played a pivotal role in establishing the current standard model.[17] New technology could improve these limits by over three

orders of magnitude, providing new insight into the history and evolution of the universe. Examples include new tests of inflation through the dissipation of primordial acoustic perturbations, searches for dark matter decay or annihilation, and the characterization of Pop III stars through Compton heating at reionization.[18–22] Recognizing the fundamental importance of precision CMB data, NASA's 2013 Astrophysics Roadmap specifically calls for new measurements of *both* CMB polarization and spectral distortions. Development of the necessary technology is a high priority, enabling the next generation of instruments to test the origins and evolution of the universe.

2. PIXIE MISSION

Recent detections of CMB polarization have, if anything, increased the urgency of new, more sensitive measurements. Figure 3 shows the angular power spectrum predicted for the inflationary B-modes and the cosmological foreground caused by gravitational lensing of the brighter E-mode signal. Several experiments have begun to map the lensing foreground on arc-minute angular scales.[23,24] The amplitude of the detected lensing signal agrees well with the standard ΛCDM cosmological model. The BICEP2 experiment has recently reported a B-mode detection at degree angular scales, consistent with an inflationary signal at unexpectedly large levels $r = 0.20$.[25] Signals at this level are difficult to reconcile with 95% CL upper limits $r < 0.11$ established by the detailed shape of unpolarized CMB anisotropy.[1,2] A primordial signal at this amplitude, if confirmed, would require modification of the standard ΛCDM model.

A key test of of the BICEP2 results is the predicted rise in power for the inflationary signal at large angular scales. BICEP2 observes the lensing signal at small angular scales, with an additional increase in power at degree angular scales. While a number of existing instruments can test the BICEP2 results on these angular scales, a space mission may be required to provide the stability and sky coverage needed to measure polarization on the largest angular scales. NASA's strategic planning includes such a space mission (the Polarization Surveyor, or CMBPol), but this mission would likely not begin formulation until the next decade, with probable launch no earlier than the late 2020's.

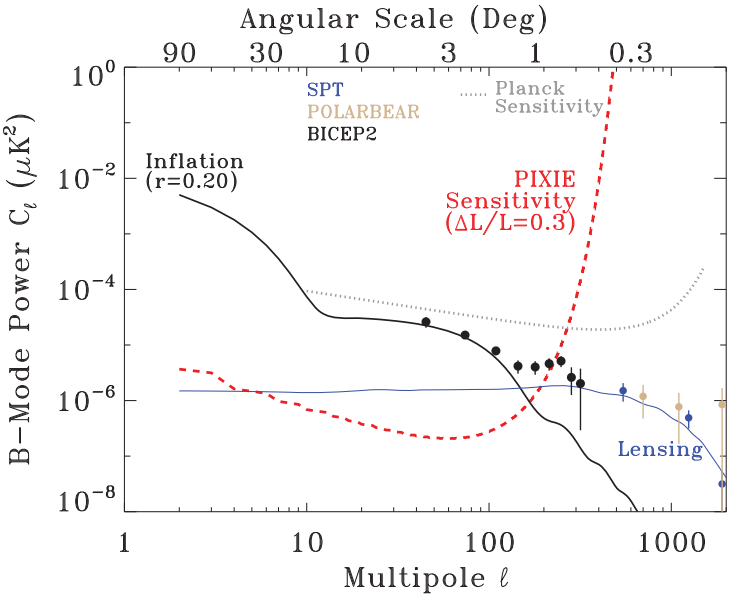

Figure 3. Recent measurements of CMB polarization are consistent with the expected lensing signal on small angular scales and an unexpectedly bright signal at degree scales. The power spectrum is consistent with inflationary models, but the amplitude $r = 0.2$ conflicts with upper limits $r < 0.11$ set by the unpolarized anisotropy. Measurements at large angular scales could detect the increased power predicted by inflationary models to provide a critical test for the origin of the detected signal.

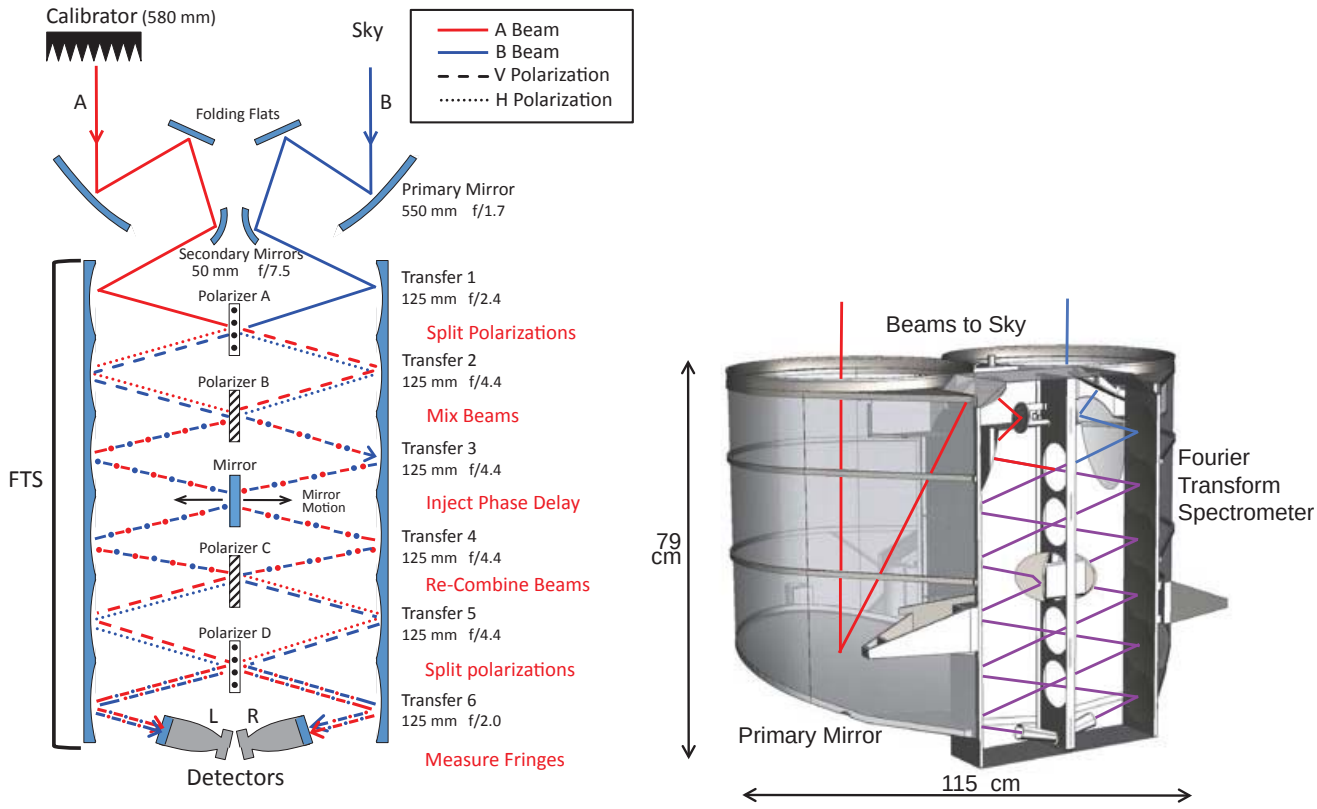

Figure 4. (Left) Schematic view of the PIXIE optical signal path. As the mirrors move, multi-moded detectors measure a fringe pattern proportional to the Fourier transform of the difference spectrum between orthogonal polarization states from the two input beams (Stokes Q in instrument coordinates). A full-aperture blackbody calibrator can move to block either input beam, or be stowed to allow both beams to view the same patch of sky. (Right) Physical layout of PIXIE optics.

The Primordial Inflation Explorer (PIXIE) is an Explorer-class mission designed to measure both the inflationary signature in polarization and the blackbody spectral distortions from more recent cosmological epochs.[26] A "light bucket" optical design provides nK sensitivity using only four multi-moded detectors. A polarizing Fourier Transform Spectrometer synthesizes 400 frequency channels across 2.5 decades to provide unparalleled separation of CMB from Galactic foregrounds. PIXIE's highly symmetric design enables nulling operation to provide the necessary control of instrumental effects. The unique design achieves breakthrough sensitivity to both polarization and spectral distortions within the resources of the existing Explorer program. As such, PIXIE could begin development at the next full Explorer call (currently anticipated for 2016 or 2017) and launch by 2023.

2.1 Instrument Description

Figure 4 shows the instrument concept. Two off-axis primary mirrors 550 mm in diameter produce twin beams co-aligned with the spacecraft spin axis. A folding flat and 50 mm secondary mirror route the beams to the FTS. A set of six transfer mirror pairs, each imaging the previous mirror to the following one, shuttles the radiation through a series of polarizing wire grids. Polarizer A transmits vertical polarization and reflects horizontal polarization, separating each beam into orthogonal polarization states. A second polarizer (B) with wires oriented 45° relative to grid A mixes the polarization states. A Mirror Transport Mechanism (MTM) moves back-to-back dihedral mirrors to inject an optical phase delay. The phase-delayed beams re-combine (interfere) at Polarizer C. Polarizer D (oriented the same as A) splits the beams again and routes them to two

multi-moded concentrator feed horns. Each concentrator is square to preserve linear polarization and contains a pair of identical bolometers, each sensitive to a single linear polarization but mounted at 90° to each other to measure orthogonal polarization states. To control stray light, all internal surfaces except the active optical elements are coated with a microwave absorber,[27] forming a blackbody cavity isothermal with the sky.

Each of the four detectors measures an interference fringe pattern between orthogonal linear polarizations from the two input beams. Let $\vec{E} = E_x\hat{x} + E_y\hat{y}$ represent the electric field incident from the sky. The power at the detectors as a function of the mirror position z may be written

$$\begin{aligned}
P_{Lx} &= 1/2 \int (E_{Ax}^2 + E_{By}^2) + (E_{Ax}^2 - E_{By}^2)\cos(4z\omega/c)d\omega \\
P_{Ly} &= 1/2 \int (E_{Ay}^2 + E_{Bx}^2) + (E_{Ay}^2 - E_{Bx}^2)\cos(4z\omega/c)d\omega \\
P_{Rx} &= 1/2 \int (E_{Ay}^2 + E_{Bx}^2) + (E_{Bx}^2 - E_{Ay}^2)\cos(4z\omega/c)d\omega \\
P_{Ry} &= 1/2 \int (E_{Ax}^2 + E_{By}^2) + (E_{By}^2 - E_{Ax}^2)\cos(4z\omega/c)d\omega \ , \qquad (7)
\end{aligned}$$

where L and R refer to the detectors in the left and right concentrators while A and B refer to the two input beams (Fig 4).

The modulated term is proportional to Fourier transform of the frequency spectrum for Stokes Q linear polarization in instrument-fixed coordinates. Rotation of the instrument about the beam axis interchanges $\hat{x}$ and $\hat{y}$ on the detectors. The sky signal then becomes

$$\begin{aligned}
S(\nu)_{Lx} &= 1/4\,[\ I(\nu)_A - I(\nu)_B + Q(\nu)_{\rm sky}\cos 2\gamma + U(\nu)_{\rm sky}\sin 2\gamma\ ] \\
S(\nu)_{Ly} &= 1/4\,[\ I(\nu)_A - I(\nu)_B - Q(\nu)_{\rm sky}\cos 2\gamma - U(\nu)_{\rm sky}\sin 2\gamma\ ] \\
S(\nu)_{Rx} &= 1/4\,[\ I(\nu)_B - I(\nu)_A + Q(\nu)_{\rm sky}\cos 2\gamma + U(\nu)_{\rm sky}\sin 2\gamma\ ] \\
S(\nu)_{Ly} &= 1/4\,[\ I(\nu)_B - I(\nu)_A - Q(\nu)_{\rm sky}\cos 2\gamma - U(\nu)_{\rm sky}\sin 2\gamma\ ] \ , \qquad (8)
\end{aligned}$$

where $I = \langle E_x^2 + E_y^2\rangle$, $Q = \langle E_x^2 - E_y^2\rangle$, and $U = 2{\rm Re}\langle E_x E_y\rangle$ are the Stokes polarization parameters, γ is the spin angle, and $S(\nu)$ denotes the synthesized frequency spectrum with bins ν set by the fringe sampling.

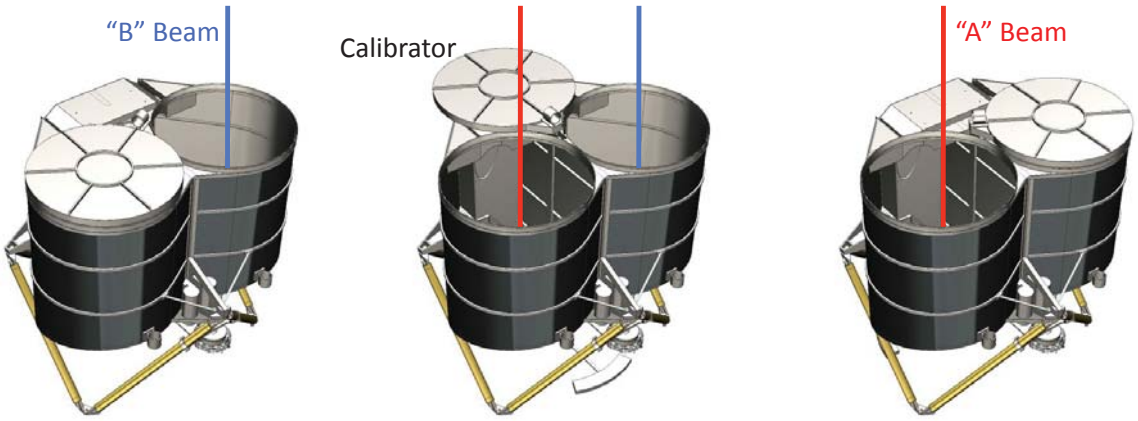

Figure 5. An external blackbody calibrator can be commanded to one of three positions: completely blocking the "A" beam (left panel), completely blocking the "B" beam (right panel), or stowed so that both beams view the sky (center). With the calibr ator stowed, PIXIE operates as a nulling polarimeter insensitive to unpolarized emission. With the calibrator deployed over either beam, PIXIE is sensitive to both polarization and spectral distortions relative to the blackbody calibrator.

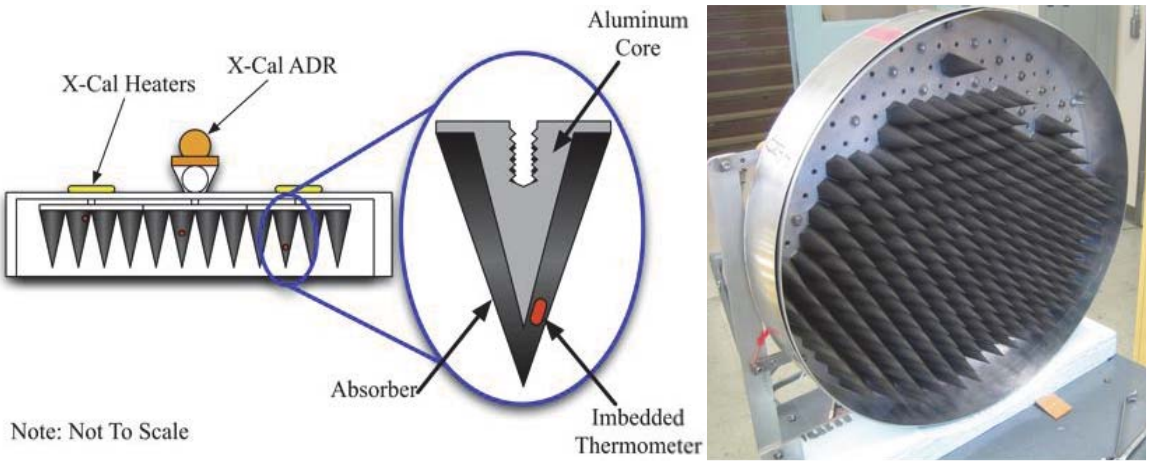

Figure 6. PIXIE calibrator design. (Left) The calibrator consists of a forest of absorbing cones mounted on a thermally conductive base. Thermometers embedded within selected cones monitor both the absolute temperature and temperature gradients. An adiabatic demagnetization refrigerator stores energy for thermal control. (Right) Photograph of the ARCADE calibrator during assembly. PIXIE uses a similar design with smaller cones to operate at shorter wavelengths.

PIXIE carries an on-board blackbody calibrator to provide an absolute reference signal The calibrator can be deployed to fully cover either one of the beams, or stowed so that both beams view the sky (Figure 5). When both beams view the sky, the instrument responds only to polarization, with the fringe pattern encoding the frequency spectrum of the polarized sky emission. When the calibrator blocks one of the beams, the fringe pattern encodes information for both polarization and the absolute intensity of the sky emission (Eq. 8).

Figure 6 shows the calibrator design. Based on the proven ARCADE calibrator,[28] it consists of 1369 absorbing cones, each 34 mm tall and 16 mm wide at the base, mounted in a close packed array on a thermally conductive aluminum plate 580 mm in diameter to fully cover one beam aperture. Each cone consists of a thermally conductive aluminum core covered with a thin absorptive skin,[27] with power reflection < -65 dB. Cernox thermometers in 39 selected cones monitor the temperature with 0.5 mK zero-point accuracy and 0.1 mK read noise per 1 sec sample. The thermometers are cast into the absorber and calibrated *in situ* against absolute temperature standards from the National Institute for Standards and Technology. The calibrator temperature can be commanded within the range 2.6–3.5 K to provide a calibration signal at frequencies below 1 THz. Calibration at frequencies above the 600 GHz CMB Wien cutoff uses a single cone heated to 20 K. The fill factor (1/1369) and temperature are chosen to approximate the spectrum of the diffuse Galactic dust cirrus.

2.2 Cryogenic Design

Figure 7 shows the cryogenic design. A combination of passive and active cooling maintains the PIXIE instrument at cryogenic temperatures. An S2 glass composite hexapod structure provides mechanical support and thermal isolation for the instrument. Four nested thermal shields provide passive cooling at 150 K while shielding the instrument against thermal emission from the Sun, Earth, and warm spacecraft. A mechanical cryocooler provides cooling from 300K to 4.5 K, with intermediate stages at 68 and 17 K. The cryocooler rejects heat to a dedicated radiator located between the outer two shields. Two adiabatic demagnetization refrigerator (ADR) systems based on the ASTRO-E2/XRS and Astro-H/SXS design cool the instrument and detectors. An instrument ADR provides a 2.6 K "thermal bus" to regulate the instrument at 2.725 K, while a second ADR provides 100 mK cooling for the detectors. The precise bus temperature is not critical; each instrument component (optics barrels, mirrors, polarizers, etc) is weakly connected to the bus to provide independent thermal control at 2.725 K. Three additional ADR stages provide a heat buffer for the external calibrator and the two input optics barrels. These buffers absorb transient loads (moonlight) over short periods and slowly push it back out to the thermal bus to be removed by the instrument ADR. By replacing peak loads with an orbital average, the buffers reduce the heat lift requirements for the cryocooler. There are no stored cryogens or other consumables, allowing operational resiliency.

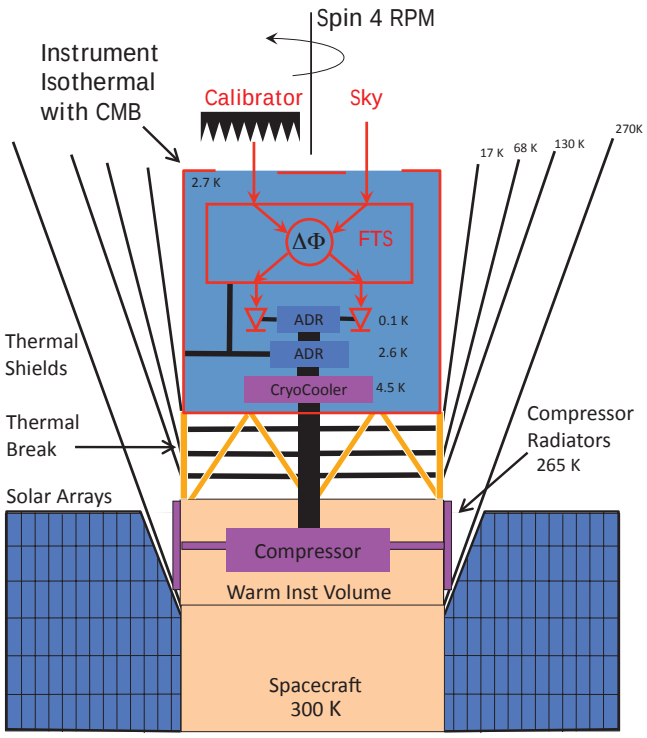

Figure 7. Cryogenic layout for the PIXIE instrument. An ADR and mechanical cryo-cooler maintain the instrument and enclosure at 2.725 K, isothermal with the CMB. A set of concentric shields surrounds the instrument to prevent heating by the Sun or Earth.

2.3 Observatory and Mission Design

Figure 8 shows the observatory and mission concept. PIXIE will launch into a 660 km polar sun-synchronous orbit with 6 AM or 6 PM ascending node to provide full-sun operation. The instrument spins at 4 RPM with the spin axis maintained 91° from the Sun line and as close as possible to the zenith consistent with the Solar pointing requirement. The instrument thus observes a great circle each orbit, while the orbit precession of 1° per day achieves full sky coverage in each 6-month observing period. The detector sampling, mirror stroke, and spacecraft spin are fast compared to the orbital motion of the beam across the sky, eliminating the need for pixel-to-pixel differences in the data analysis.

PIXIE is a technologically mature small mission, well within the capabilities of NASA's Explorer program. Figure 9 shows the observatory in launch configuration. The observatory size is set by the two 55 cm primary mirrors, and fits easily within the 92" fairing of either the Taurus, Athena, or comparable launch vehicle.

3. INSTRUMENT PERFORMANCE

PIXIE's innovative optical design combines multi-moded optics with a Fourier Transform Spectrometer to provide breakthrough sensitivity for CMB polarimetry using only four semiconductor detectors. The design addresses each of the principal challenges for CMB polarimetry. A multi-moded "light bucket" provides nK sensitivity using only four detectors. A polarizing Fourier Transform Spectrometer (FTS) synthesizes 400 channels across 2.5 decades in frequency to provide unparalleled separation of CMB from Galactic foregrounds. PIXIE's highly symmetric design enables operation as a nulling polarimeter to provide the necessary control of instrumental effects.

3.1 Sensitivity

PIXIE uses muti-moded optics to achieve background-limited sensitivity with only 4 detectors. The noise equivalent power (NEP) of photon noise in a single linear polarization is given by

$$\mathrm{NEP}^2_{\mathrm{photon}} = \frac{2A\Omega}{c^2}\frac{(kT)^5}{h^3}\int \alpha\epsilon f \ \frac{x^4}{e^x-1}\ \left(1+\frac{\alpha\epsilon f}{e^x-1}\right)\ dx, \tag{9}$$

where A is the detector area, Ω is the detector solid angle, α is detector absorptivity, T is the physical temperature of the source, ϵ is the emissivity of the source, and f is the power transmission through the optics.[29] For a fixed integration time τ the detected noise is simply

$$\delta P = \frac{\mathrm{NEP}}{\sqrt{\tau/2}} \tag{10}$$

where the factor of 2 accounts for the conversion between the frequency and time domains. The noise at the detector may in turn be referred to the specific intensity on the sky,

$$\delta I_\nu = \frac{\delta P}{A\Omega\ \Delta\nu\ (\alpha\epsilon f)} \tag{11}$$

where $\Delta\nu$ is the observing bandwidth.

PIXIE combines a large collecting area with non-imaging optics to maximize the number of photons while minimizing the detector count. The light-gathering ability of an instrument is specified by its etendu $A\Omega$. Increasing the etendu for a single detector increases the photon noise, NEP $\propto$ $(A\Omega)^{1/2}$. But since the signal increases linearly with etendu, the signal-to-noise ratio *improves* as $(A\Omega)^{1/2}$.

The multi-moded PIXIE optics provide sensitivity comparable to kilo-pixel focal plane arrays while requiring only 4 semiconductor bolometers. For diffraction-limited single-mode optics, the etendu and wavelength are

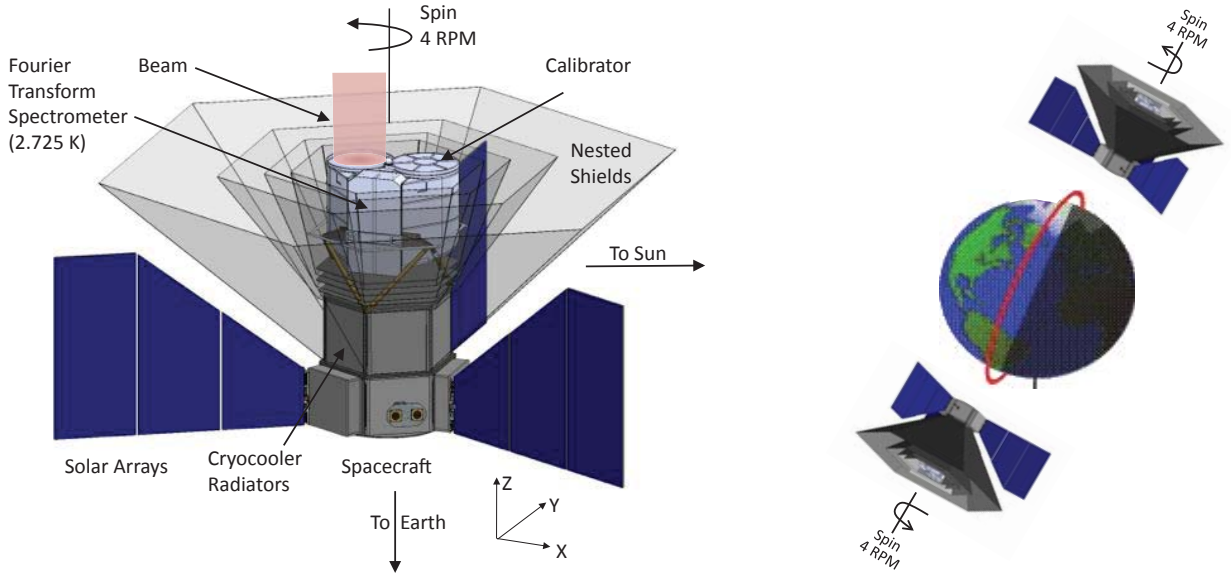

Figure 8. PIXIE observatory and mission concept. The instrument is maintained at 2.725 K and is surrounded by shields to block radiation from the Sun or Earth. It observes from a 660 km polar sun-synchronous terminator orbit. The rapid spin and interferometer stroke efficiently separate Stokes I, Q, and U parameters independently within each pixel to provide a nearly diagonal covariance matrix.

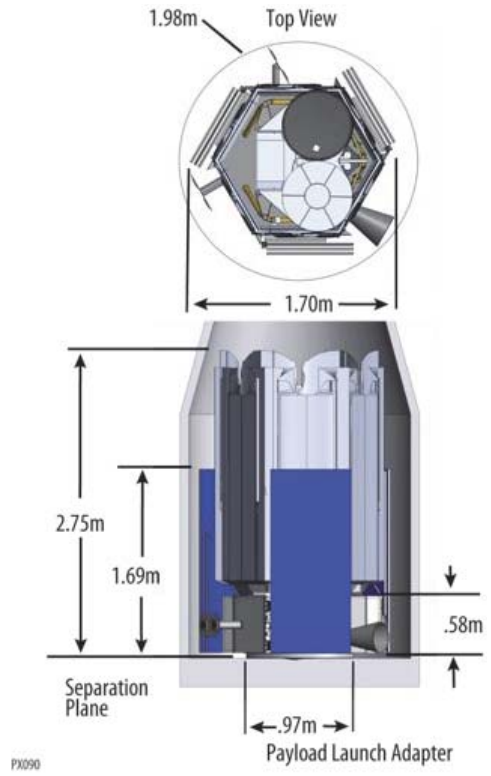

Figure 9. The PIXIE observatory fits easily within the Explorer 92" fairing.

related as $A\Omega = \lambda^2$ so that the beam size scales with the observing wavelength. For multi-moded optics, however, the beam size is fixed and the number of modes N scales as $N = A\Omega/\lambda^2$. Multi moded optics thus allow a considerable increase in sensitivity compared to single-moded designs of comparable size. The improvement is large enough to allow precision measurement of the gravity-wave signature in polarization using a handful of detectors. Over just the frequency range 30–600 GHz where the CMB is brightest, each PIXIE detector measures 22,000 independent modes of the electric field.

With the calibrator deployed over either aperture, the instrument measures both polarized and unpolarized emission (Stokes I, Q, and U). With both beams open to the sky, the instrument is insensitive to unpolarized emission but has twice the sensitivity to polarized signals*. Averaging over the four detectors, the combined instrument sensitivity to either unpolarized or polarized emission within each synthesized frequency bin is

$$\begin{aligned} \delta I_\nu^I &= 2.4 \times 10^{-22} \text{ W m}^{-2} \text{ sr}^{-1} \text{ Hz}^{-1} \\ \delta I_\nu^{QU} &= 3.4 \times 10^{-22} \text{ W m}^{-2} \text{ sr}^{-1} \text{ Hz}^{-1} \end{aligned} \quad (12)$$

for a one-second integration with the calibrator deployed over either aperture, and

$$\delta I_\nu^{QU} = 0.5 \times 10^{-22} \text{ W m}^{-2} \text{ sr}^{-1} \text{ Hz}^{-1} \quad (13)$$

when the calibrator is stowed.[26] PIXIE will spend approximately 30% of the observing time with the calibrator deployed and 60% with the calibrator stowed. The remaining 10% includes both high-temperature calibration of the Galactic dust signal and lost observing time.

*Replacing the blackbody calibrator emission with sky emission in one beam leaves the noise nearly unchanged but doubles the sky signal incident on the FTS.

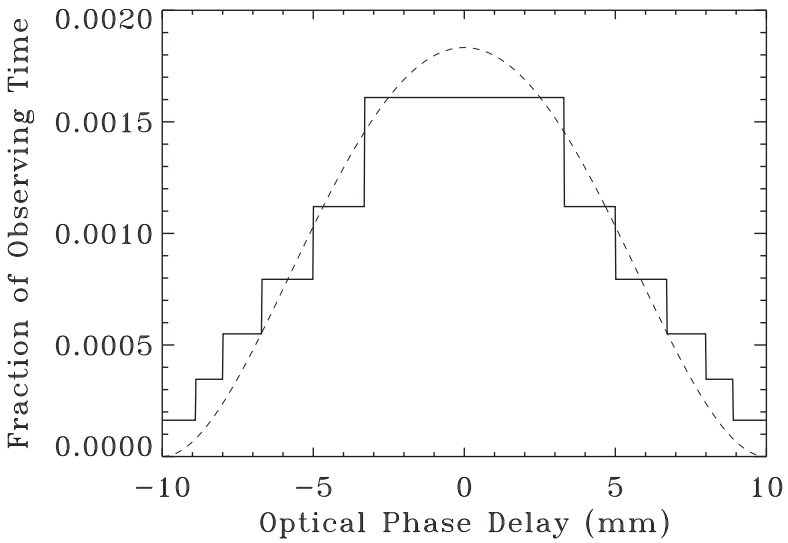

Figure 10. Apodization of the optical phase delay ΔL created by scanning the dihedral mirror through different physical stroke lengths on different orbits. The achieved apodization (solid line) closely approximates the ideal (dashed line).

3.2 Frequency Channels

The fringe pattern measured at each detector samples the Fourier transform of the frequency spectrum of the difference between one linear polarization from the A-side beam and the orthogonal linear polarization from the B-side beam (Eq. 7). The frequency bins in the synthesized spectra $S(\nu)$ are set by the mirror throw and detector sampling,

$$S_\nu = \sum_{k=0}^{N_s-1} S_i \exp(2\pi i \nu k/N_s) \tag{14}$$

where S_i is a time-ordered sample and ν denotes frequency. As the mirror moves, we obtain N_s detector samples over an optical path length $\pm\Delta L$. The Fourier transform of the sampled fringe pattern returns frequencies $n \times c/(2\Delta L)$ where $n = 0, 1, 2, ..., N_s/2$. The path length (optical stroke) thus determines the width of the frequency bins in the synthesized spectra, while the number of detector samples within each optical stroke determines the number of frequency bins and thus the highest sampled frequency. For nominal operation we plan $N_s = 1024$ and $\Delta L = 1$ cm, to obtain 512 synthesized frequency bins of width 15 GHz each. The corresponding physical mirror movement $\Delta z = \Delta L/[4\cos(\alpha)\cos(\delta/2)] = \pm 2.58$ mm accounts for the folded optics as well as the off-axis optical path ($\alpha = 15°$) and beam divergence within the FTS ($\delta = 6.5°$).

The mirror is under active control. Both the stroke length and sampling can be adjusted in flight to modify the channel width or number of channels. PIXIE's minimum channel width $\Delta\nu = 15$ GHz is set by the maximum physical path length and provides modest spectral resolution $\nu/\Delta\nu \sim 100$ for lines at THz frequencies. Using a shorter mirror stroke provides wider synthesized channels with correspondingly higher signal to noise ratio for continuum emission. Note that once the stroke length ΔL is set to determine the channel width, there is essentially no penalty (other than data storage) for extending observations to higher frequencies by increasing the number of data samples N_s. The practical limit is set by several factors. The beams within the FTS are not plane waves but use collimating optics with half-angle 6.°5. The resulting dispersion causes loss of fringe coherence at short wavelengths. The optical polarizers use wire grids, which become inefficient in reflection at wavelengths shorter than twice the 30 μm wire pitch, further reducing the fringe amplitude. These effects combine to limit the effective frequency range to $\nu < 6$ THz: although the nominal synthesized spectra have 512 channels to a maximum of 7665 GHz, channels at frequencies above 6 THz (wavelength 50 μm) will have little

Table 1. Mirror Apodization Sampling

Orbit Number	Optical Delay	Physical Stroke	Samples per Stroke
1 & 2	±10 mm	±2.6 mm	1024
3 & 4	±8.9 mm	±2.3 mm	910
5 & 6	±8.0 mm	±2.1 mm	819
7 & 8	±6.7 mm	±1.7 mm	683
9 & 10	±5.0 mm	±1.3 mm	512
11 & 12	±3.3 mm	±0.9 mm	341

sensitivity to sky signal[†]

Active control of the mirror stroke also enables near ideal apodization of the observed fringe pattern. A Fourier transform uniformly sampled from -1 to +1 has sharp edges at ±1, leading to ringing in the frequency domain. In addition, the CMB only produces fringes near zero path length — observations at longer optical path, necessary to provide sufficiently narrow frequency bins, have little CMB signal and contribute little to the CMB sensitivity. We minimize ringing and maximize sensitivity by varying the mirror stroke to apodize the Fourier transform. This softens the edges in the position domain by spending less time observing at large optical path length, while maximizing CMB sensitivity by spending more time observing CMB fringes near the optical null. A commonly used apodization is $(1-z^2)^2$. We approximate this apodization by varying the mirror stroke length on successive orbits. PIXIE observes the sky from a polar sun-synchronous orbit. The orbit plane precesses 1° per day, so that a pixel near the celestial equator is visible for at least 13 consecutive orbits. Each orbit uses a different mirror stroke length, ranging from shortest stroke $\Delta z = \pm 0.86$ mm (optical path length $\Delta L = \pm 3.3$ mm) to a longest stroke $\Delta z = \pm 2.58$ mm (optical path length $\Delta L = \pm 10.0$ mm). Table 3.2 summarizes the mirror stroke pattern. The resulting apodization closely approximates the ideal (Figure 10). Optical paths near zero delay are observed much more often than paths at large delay, and have correspondingly smaller noise, while optical paths at large phase delay are seldom observed and have larger noise. Simulations of the Fourier transform using this non-uniform noise pattern show noise in the Fourier transform to be smaller by a factor 0.73 compared to simulations with the equivalent integration time and no apodization.

Figure 11 summarizes the sensitivity and frequency coverage. PIXIE will observe in 400 frequency channels each 15 Ghz wide, ranging from 30 GHz to 6 THz to distinguish primordial signals from Galactic foregrounds. Eqs 12 and 13 give the specific intensity within each synthesized frequency bin. For continuum sources like the CMB we may integrate over multiple bins to further improve sensitivity. A 4-year mission achieves rms sensitivity 70 nK within each $1^\circ \times 1^\circ$ pixel. Averaged over the cleanest 75% of the sky, PIXIE will characterize the gravity-wave signal at sensitivity $\delta r = 2 \times 10^{-4}$ (68% CL). The resulting sensitivity allows characterization of the B-mode angular power spectrum $\ell < 200$ to allow overlap with measurements by ground-based instruments observing on smaller angular scales (Figure 3).

3.3 Systematic Errors

PIXIE operates as a nulling polarimeter: the fringe pattern from the FTS depends only on the *difference* between two beams viewing nearly identical sources. The resulting null operation greatly reduces sensitivity to systematic errors. In addition, the highly symmetric design provides multiple levels of rejection for potential instrumental effects. Each detector measures the difference between the $\hat{x}$ polarization from one beam and the $\hat{y}$ polarization from the other beam. The four detectors thus sample different combinations of $\hat{x}$ vs $\hat{y}$ polarization from the A vs B beams in the left vs right optics (Eq. 7). Common-mode instrumental effects cancel in the appropriate sum or difference of selected detector pairs. Residual drifts or $1/f$ noise in the time domain, which typically induce map striping in conventional radiometers, are Fourier transformed into the frequency domain and only

[†]Photon noise from emission at high frequencies should also be considered. Thermal emission from the diffuse 20 K dust cirrus does not contribute significantly to the noise budget, but emission from zodiacal dust would degrade sensitivity. Such high-frequency noise contributions can not be reduced by the mirror sampling but require hardware solutions such as a low-pass filter. The PIXIE optics include a low-pass filter with a kne at 100 μm to block short-wavelength emission.

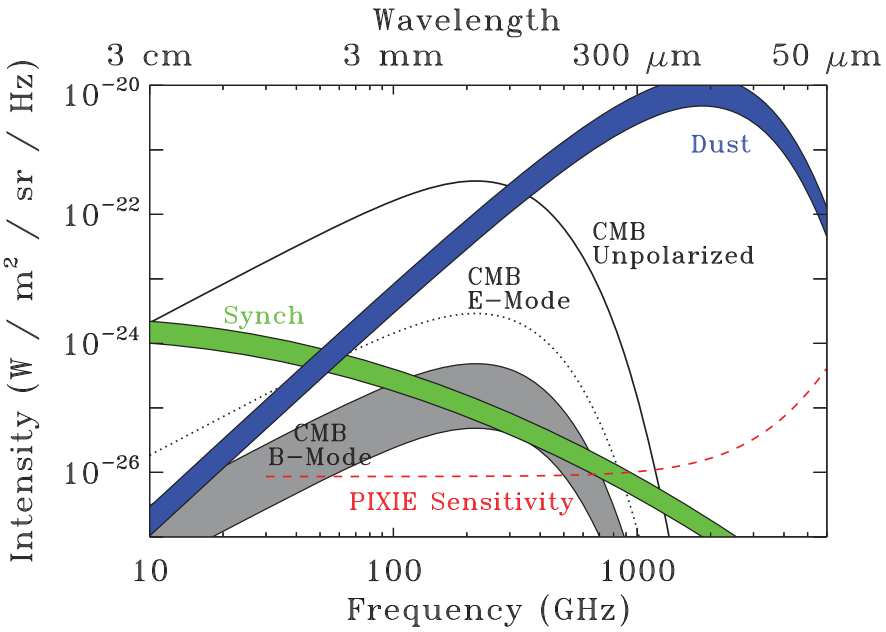

Figure 11. RMS anisotropy for the CMB and polarized foregrounds. The dashed line shows the rms noise within each synthesized frequency channel, averaged over the high-latitude sky. The grey band shows the range of amplitudes $0.01 < r < 0.1$ for the primordial gravity-wave signal. The width of the dust and synchrotron bands reflects rms foreground variation along high-latitude lines of sight. PIXIE combines multi-moded optics with a Fourier Transform Spectrometer to achieve high sensitivity in 400 spectral channels spanning 2.5 decades in frequency.

affect the lowest few bins of the synthesized spectra. The fringe pattern observed as the mirror moves from one endpoint through the white-light null to the other endpoint modulates sky signals on time scales from 1 ms to 1 s (Figure 12). True sky signals are independent of the sign (near vs far side of null) and direction (forward vs back) of the mirror motion, allowing clean separation of sky signal from instrumental effects (detector time constant, responsivity).

The PIXIE design has additional guards against instrumental effects. Unlike simple polarization-sensitive detectors, where instrument rotation produces a sinusoidal response to polarized sky signals, rotating the PIXIE instrument produces amplitude modulation of the *entire fringe pattern* at twice the spin frequency (Fig 12). The resulting modulated fringe pattern is readily distinguished from a simple spin-locked sine wave or its harmonics, suppressing spin-synchronous drifts.

PIXIE provides robust discrimination against systematic errors even allowing for typical fabrication tolerances. Mathematically exact cancellation of competing signals is not required. Consider, for example, the effects of non-ideal optical performance. Differences in the transmission, reflection, and absorption coefficients within the instrument drive the response away from the ideal null behavior. Such effects are small and readily identified. Let radiation $\vec{E}_0 = E_x\hat{x} + E_y\hat{y}$ be incident on the first polarizing grating (polarizer A in Fig. 4). The grating reflects $\hat{y}$ and transmits $\hat{x}$. The reflected beam is $\vec{E}_r = -E_y\hat{y}$ and the transmitted beam is $\vec{E}_t = [(1-\alpha)E_x + \alpha E_g]\hat{x}$ where $\alpha \sim 0.05$ is the absorption coefficient of the grating and for simplicity we assume that absorption applies only in a single linear polarization. E_g is the amplitude of the electric field emitted by the grating in the $\hat{x}$ polarization and is proportional to the blackbody intensity at the grating physical temperature. The absorption term drives the polarimeter off null, creating a fringe response to unpolarized sky emission. The resulting systematic error terms may be written

$$\begin{aligned} \Delta S(\nu)_{Lx} &= 1/4\left[-\alpha^2(Q_\nu \cos 2\gamma + U_\nu \sin 2\gamma) + \alpha^2 \Delta I_\nu\right] \\ \Delta S(\nu)_{Ry} &= 1/4\left[\ \alpha^2(Q_\nu \cos 2\gamma + U_\nu \sin 2\gamma) - \alpha^2 \Delta I_\nu\right] \end{aligned} \quad (15)$$

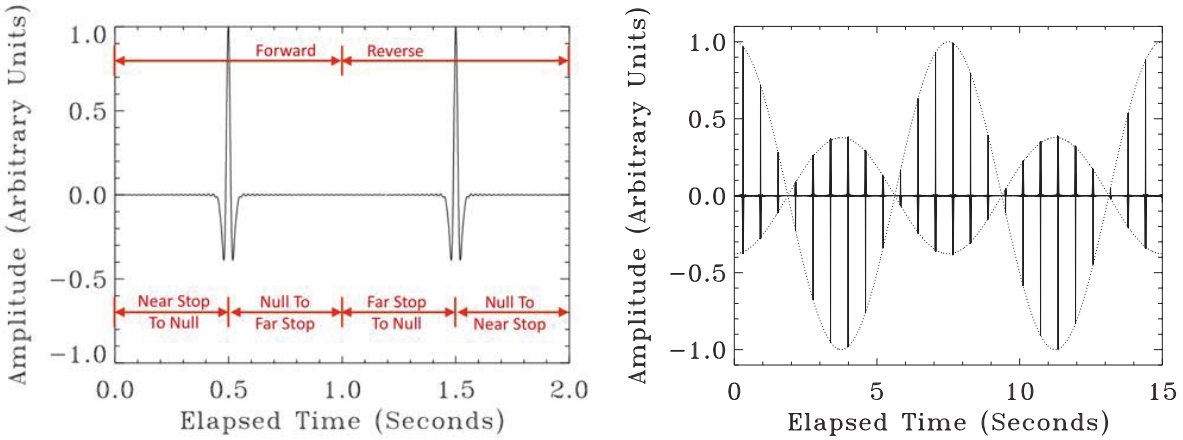

Figure 12. (Left) Simulated fringe pattern from a single detector observing a CMB source as the mirror scans through a complete cycle. Sky signals must follow multiple space- and time-reversal symmetries, allowing straightforward subtraction of instrumental signals. (Right) Fringe pattern from a polarized source for one complete spin period (shown here with mirror period 0.6 sec and spin period 15 sec). Sky rotation imposes an amplitude modulation on the entire fringe pattern to distinguish sky polarization from instrumental effects.

where S_ν are the synthesized frequency spectra for the $\hat{x}$ detector in the left feed and the $\hat{y}$ detector in the right feed, respectively (similar terms apply for the other two detectors). The first term is proportional to the sky polarization, and represents a correction to the instrument calibration to account for loss in the optics. Its amplitude is small (< 2 nK).

4. SCIENCE GOALS

PIXIE will map the full sky in absolute intensity and linear polarization (Stokes I, Q, and U) with angular resolution $2\overset{\circ}{.}6$ in each of 400 frequency channels 15 GHz wide from 30 GHz to 6 THz. The calibrated spectral data at each frequency will be binned into 49152 sky pixels each $0\overset{\circ}{.}9$ in diameter using the HEALPIX pixelization.[30] Typical sensitivities within each mid-latitude pixel are

$$\delta I_\nu^I = 4 \times 10^{-24} \text{ W m}^{-2} \text{ s}^{-1} \text{ sr}^{-1} \tag{16}$$

for Stokes I and

$$\delta I_\nu^{QU} = 6 \times 10^{-25} \text{ W m}^{-2} \text{ s}^{-1} \text{ sr}^{-1} \tag{17}$$

for Stokes Q or U. The resulting data set supports a broad range of science goals.

- **CMB Polarization** PIXIE will map CMB polarization to sensitivity 70 nK per $1^\circ \times 1^\circ$ pixel. PIXIE will map the gravitational signature of inflation at sensitivity $\delta r = 2 \times 10^{-4}$, allowing percent-level characterization of the inflationary signal even if the amplitude is as small as $r \sim 0.02$.
- **Spectral Distortions** PIXIE will compare the sky to a full-aperture calibrator to map deviations from a blackbody spectrum. Multiple symmetries within the instrument allow clean identification of instrumental signatures, providing 68% confidence limits $|\mu| < 10^{-8}$ for a chemical potential distortion and $|y| < 2 \times 10^{-9}$ for a Compton distortion. Measurements at these sensitivities probe a variety of physical processes in the early universe, including dissipation of primordial density perturbations, decay or annihilation of dark matter, primordial black holes, the physics of recombination, and the nature of the first collapsed objects at reionization.[31]
- **Star Formation History** The cosmic infrared background (CIB) results from cumulative emission from dusty galaxies since their epoch of formation, providing an integral constraint on the star formation history

Table 2. Selected Line Emission From the Interstellar Medium

Molecular Gas		Photodissociation Regions		HII Regions		Hot ($T > 10^5$ K) Gas	
CO $1 \rightarrow 0$	115 GHz	FeII	51.3, 87.4 μm	FeIII	51.7 μm	OIII	51.8 μm
CO $2 \rightarrow 1$	231 GHz	FeI	54.3, 111.2 μm	NIII	57.3 μm	NIII	57.3 μm
CO $30 \rightarrow 29$	3438 GHz	SI	56.3 μm	FeII	87.4 μm	FeV	70.4 μm
H_2O	22 GHz	OI	63.2 μm	FeIII	105.4 μm	OIII	88.4 μm
H_2O	183 GHz	SiII	68.5, 129.7 μm	NII	121.9 μm		
CS $1 \rightarrow 0$	49 GHz	OI	145.5 μm	SiII	129.7 μm		
CS $2 \rightarrow 1$	98 GHz	CII	157.7 μm	NII	205.2 μm		
CS $4 \rightarrow 3$	196 GHz	CI	370.4, 609.1 μm				

of the universe. The absolute emission spectrum as a function of angular scale is sensitive to the entire history of dusty star-forming galaxies.[32] Spatial fluctuations in the CIB should correlate with the integrated Sachs-Wolfe effect and gravitational lensing fluctuations.[33] The combination is a powerful probe of the characteristic mass of star-forming galaxies and the integrated cosmic star formation history. PIXIE's sensitivity at large angular scales over a broad range of frequencies spanning the peak CIB intensity will complement measurements by Herschel, Planck, and other observatories.

- **Interstellar Medium** PIXIE's all-sky spectral cubes provide important insights into the interstellar medium (ISM) within the Galaxy. Thermal emission from dust within our galaxy dominates the far-infrared sky brightness. Dust emission is partially polarized by magnetic alignment of aspherical grains PIXIE can measure the spectral index of both polarized and unpolarized dust emission to better than 0.1% precision within each 1° pixel to distinguish models of dust emission mechanism and chemical composition. In addition, PIXIE will map far-IR line emission from both molecular and atomic species to characterize the temperature, density, and radiation fields within distinct phases of the interstellar medium (Table 2).

PIXIE's primary goals are to characterize primordial inflation through the signature in CMB polarization, and to constrain energetic processes in the early universe through measurements of spectral distortions. These goals reflect priorities outlined in the 2010 *New Worlds, New Horizons* Astrophysics Decadal Survey and further endorsed by NASA's Astrophysics Roadmap *Enduring Quests, Daring Visions*.[34] PIXIE is technologically mature and can achieve these goals within the resources of the existing Explorer program.

REFERENCES

1. Hinshaw, G., Larson, D., Komatsu, E., Spergel, D. N., Bennett, C. L., Dunkley, J., Nolta, M. R., Halpern, M., Hill, R. S., Odegard, N., Page, L., Smith, K. M., Weiland, J. L., Gold, B., Jarosik, N., Kogut, A., Limon, M., Meyer, S. S., Tucker, G. S., Wollack, E., and Wright, E. L., "Nine-year Wilkinson Microwave Anisotropy Probe (WMAP) Observations: Cosmological Parameter Results," *The Astrophysical Journal* **208**, 19 (Oct. 2013).
2. Planck Collaboration, Ade, P. A. R., Aghanim, N., Armitage-Caplan, C., Arnaud, M., Ashdown, M., Atrio-Barandela, F., Aumont, J., Baccigalupi, C., Banday, A. J., and et al., "Planck 2013 results. XVI. Cosmological parameters," *ArXiv e-prints* (Mar. 2013).
3. Keisler, R., Reichardt, C. L., Aird, K. A., Benson, B. A., Bleem, L. E., Carlstrom, J. E., Chang, C. L., Cho, H. M., Crawford, T. M., Crites, A. T., de Haan, T., Dobbs, M. A., Dudley, J., George, E. M., Halverson, N. W., Holder, G. P., Holzapfel, W. L., Hoover, S., Hou, Z., Hrubes, J. D., Joy, M., Knox, L., Lee, A. T., Leitch, E. M., Lueker, M., Luong-Van, D., McMahon, J. J., Mehl, J., Meyer, S. S., Millea, M., Mohr, J. J., Montroy, T. E., Natoli, T., Padin, S., Plagge, T., Pryke, C., Ruhl, J. E., Schaffer, K. K., Shaw, L., Shirokoff, E., Spieler, H. G., Staniszewski, Z., Stark, A. A., Story, K., van Engelen, A., Vanderlinde, K., Vieira, J. D., Williamson, R., and Zahn, O., "A Measurement of the Damping Tail of the Cosmic Microwave Background Power Spectrum with the South Pole Telescope," *The Astrophysical Journal* **743**, 28 (Dec. 2011).

4. Rubakov, V. A., Sazhin, M. V., and Veryaskin, A. V., "Graviton creation in the inflationary universe and the grand unification scale," *Physics Letters B* **115**, 189–192 (Sept. 1982).
5. Fabbri, R. and Pollock, M. D., "The effect of primordially produced gravitons upon the anisotropy of the cosmological microwave background radiation," *Physics Letters B* **125**, 445–448 (June 1983).
6. Abbott, L. F. and Wise, M. B., "Constraints on generalized inflationary cosmologies," *Nuclear Physics B* **244**, 541–548 (Oct. 1984).
7. Polnarev, A. G., "Polarization and anisotropy induced in the microwave background by cosmological gravitational waves," *Astronomicheskii Zhurnal* **62**, 1041–1052 (Dec. 1985).
8. Davis, R. L., Hodges, H. M., Smoot, G. F., Steinhardt, P. J., and Turner, M. S., "Cosmic microwave background probes models of inflation," *Physical Review Letters* **69**, 1856–1859 (Sept. 1992).
9. Grishchuk, L. P., "Cosmological perturbations of quantum-mechanical origin and anisotropy of the microwave background," *Physical Review Letters* **70**, 2371–2374 (Apr. 1993).
10. Kamionkowski, M., Kosowsky, A., and Stebbins, A., "Statistics of cosmic microwave background polarization," *Physcal Review D* **55**, 7368–7388 (June 1997).
11. Seljak, U. and Zaldarriaga, M., "Signature of Gravity Waves in the Polarization of the Microwave Background," *Physical Review Letters* **78**, 2054–2057 (Mar. 1997).
12. Illarionov, A. F. and Siuniaev, R. A., "Comptonization, the spectrum of RELICT radiation, and the thermal history of the universe," *Astronomicheskii Zhurnal* **51**, 1162–1176 (Dec. 1974).
13. Burigana, C., Danese, L., and de Zotti, G., "Formation and evolution of early distortions of the microwave background spectrum - A numerical study," *Astronomy & Astrophysics* **246**, 49–58 (June 1991).
14. Zeldovich, Y. B. and Sunyaev, R. A., "The Interaction of Matter and Radiation in a Hot-Model Universe," *Astrophysics and Space Science* **4**, 301–316 (July 1969).
15. Chluba, J. and Sunyaev, R. A., "The evolution of CMB spectral distortions in the early Universe," *Monthly Notices of the Royal Astronomical Society* **419**, 1294–1314 (Jan. 2012).
16. Chluba, J. and Jeong, D., "Teasing bits of information out of the CMB energy spectrum," *Monthly Notices of the Royal Astronomical Society* **438**, 2065–2082 (Mar. 2014).
17. Fixsen, D. J. and Mather, J. C., "The Spectral Results of the Far-Infrared Absolute Spectrophotometer Instrument on COBE," *The Astrophysical Journal* **581**, 817–822 (Dec. 2002).
18. Daly, R. A., "Spectral distortions of the microwave background radiation resulting from the damping of pressure waves," *The Astrophysical Journal* **371**, 14–28 (Apr. 1991).
19. Hu, W., Scott, D., and Silk, J., "Power spectrum constraints from spectral distortions in the cosmic microwave background," *The Astrophysical Journall* **430**, L5–L8 (July 1994).
20. Silk, J. and Stebbins, A., "Decay of long-lived particles in the early universe," *The Astrophysical Journal* **269**, 1–12 (June 1983).
21. McDonald, P., Scherrer, R. J., and Walker, T. P., "Cosmic microwave background constraint on residual annihilations of relic particles," *Physical Review D* **63**, 023001 (Jan. 2001).
22. Feng, J. L., Rajaraman, A., and Takayama, F., "Superweakly interacting massive particle dark matter signals from the early Universe," *Physical Review D* **68**, 063504 (Sept. 2003).
23. Hanson, D., Hoover, S., Crites, A., Ade, P. A. R., Aird, K. A., Austermann, J. E., Beall, J. A., Bender, A. N., Benson, B. A., Bleem, L. E., Bock, J. J., Carlstrom, J. E., Chang, C. L., Chiang, H. C., Cho, H.-M., Conley, A., Crawford, T. M., de Haan, T., Dobbs, M. A., Everett, W., Gallicchio, J., Gao, J., George, E. M., Halverson, N. W., Harrington, N., Henning, J. W., Hilton, G. C., Holder, G. P., Holzapfel, W. L., Hrubes, J. D., Huang, N., Hubmayr, J., Irwin, K. D., Keisler, R., Knox, L., Lee, A. T., Leitch, E., Li, D., Liang, C., Luong-Van, D., Marsden, G., McMahon, J. J., Mehl, J., Meyer, S. S., Mocanu, L., Montroy, T. E., Natoli, T., Nibarger, J. P., Novosad, V., Padin, S., Pryke, C., Reichardt, C. L., Ruhl, J. E., Saliwanchik, B. R., Sayre, J. T., Schaffer, K. K., Schulz, B., Smecher, G., Stark, A. A., Story, K. T., Tucker, C., Vanderlinde, K., Vieira, J. D., Viero, M. P., Wang, G., Yefremenko, V., Zahn, O., and Zemcov, M., "Detection of B-Mode Polarization in the Cosmic Microwave Background with Data from the South Pole Telescope," *Physical Review Letters* **111**, 141301 (Oct. 2013).

24. The POLARBEAR Collaboration, Ade, P. A. R., Akiba, Y., Anthony, A. E., Arnold, K., Atlas, M., Barron, D., Boettger, D., Borrill, J., Chapman, S., Chinone, Y., Dobbs, M., Elleflot, T., Errard, J., Fabbian, G., Feng, C., Flanigan, D., Gilbert, A., Grainger, W., Halverson, N. W., Hasegawa, M., Hattori, K., Hazumi, M., Holzapfel, W. L., Hori, Y., Howard, J., Hyland, P., Inoue, Y., Jaehnig, G. C., Jaffe, A. H., Keating, B., Kermish, Z., Keskitalo, R., Kisner, T., Le Jeune, M., Lee, A. T., Leitch, E. M., Linder, E., Lungu, M., Matsuda, F., Matsumura, T., Meng, X., Miller, N. J., Morii, H., Moyerman, S., Myers, M. J., Navaroli, M., Nishino, H., Paar, H., Peloton, J., Poletti, D., Quealy, E., Rebeiz, G., Reichardt, C. L., Richards, P. L., Ross, C., Schanning, I., Schenck, D. E., Sherwin, B. D., Shimizu, A., Shimmin, C., Shimon, M., Siritanasak, P., Smecher, G., Spieler, H., Stebor, N., Steinbach, B., Stompor, R., Suzuki, A., Takakura, S., Tomaru, T., Wilson, B., Yadav, A., and Zahn, O., "A Measurement of the Cosmic Microwave Background B-Mode Polarization Power Spectrum at Sub-Degree Scales with POLARBEAR," *ArXiv e-prints* (Mar. 2014).
25. BICEP2 Collaboration, Ade, P. A. R., Aikin, R. W., Barkats, D., Benton, S. J., Bischoff, C. A., Bock, J. J., Brevik, J. A., Buder, I., Bullock, E., Dowell, C. D., Duband, L., Filippini, J. P., Fliescher, S., Golwala, S. R., Halpern, M., Hasselfield, M., Hildebrandt, S. R., Hilton, G. C., Hristov, V. V., Irwin, K. D., Karkare, K. S., Kaufman, J. P., Keating, B. G., Kernasovskiy, S. A., Kovac, J. M., Kuo, C. L., Leitch, E. M., Lueker, M., Mason, P., Netterfield, C. B., Nguyen, H. T., O'Brient, R., Ogburn, IV, R. W., Orlando, A., Pryke, C., Reintsema, C. D., Richter, S., Schwarz, R., Sheehy, C. D., Staniszewski, Z. K., Sudiwala, R. V., Teply, G. P., Tolan, J. E., Turner, A. D., Vieregg, A. G., Wong, C. L., and Yoon, K. W., "BICEP2 I: Detection Of B-mode Polarization at Degree Angular Scales," *ArXiv e-prints* (Mar. 2014).
26. Kogut, A., Fixsen, D. J., Chuss, D. T., Dotson, J., Dwek, E., Halpern, M., Hinshaw, G. F., Meyer, S. M., Moseley, S. H., Seiffert, M. D., Spergel, D. N., and Wollack, E. J., "The Primordial Inflation Explorer (PIXIE): a nulling polarimeter for cosmic microwave background observations," *Journal of Cosmology and Astroparticle Physics* **7**, 25 (July 2011).
27. Wollack, E. J., Fixsen, D. J., Henry, R., Kogut, A., Limon, M., and Mirel, P., "Electromagnetic and Thermal Properties of a Conductively Loaded Epoxy," *International Journal of Infrared and Millimeter Waves* **29**, 51–61 (Jan. 2008).
28. Fixsen, D. J., Wollack, E. J., Kogut, A., Limon, M., Mirel, P., Singal, J., and Fixsen, S. M., "Compact radiometric microwave calibrator," *Review of Scientific Instruments* **77**, 064905 (June 2006).
29. Mather, J. C., "The Cosmic Background Explorer /COBE/," *Optical Engineering* **21**, 769–774 (Aug. 1982).
30. Górski, K. M., Hivon, E., Banday, A. J., Wandelt, B. D., Hansen, F. K., Reinecke, M., and Bartelmann, M., "HEALPix: A Framework for High-Resolution Discretization and Fast Analysis of Data Distributed on the Sphere," *The Astrophysical Journal* **622**, 759–771 (Apr. 2005).
31. Chluba, J., "Science with CMB spectral distortions," *ArXiv e-prints* (May 2014).
32. Knox, L., Cooray, A., Eisenstein, D., and Haiman, Z., "Probing Early Structure Formation with Far-Infrared Background Correlations," *The Astrophysical Journal* **550**, 7–20 (Mar. 2001).
33. Cooray, A., Eales, S., Chapman, S., Clements, D. L., Dore, O., Farrah, D., Jarvis, M. J., Kaplinghat, M., Negrello, M., Melchiorri, A., and et al., "The Herschel-SPIRE Legacy Survey (HSLS): the scientific goals of a shallow and wide submillimeter imaging survey with SPIRE," *ArXiv e-prints* (July 2010).
34. Kouveliotou, C., Agol, E., Batalha, N., Bean, J., Bentz, M., Cornish, N., Dressler, A., Figueroa-Feliciano, E., Gaudi, S., Guyon, O., Hartmann, D., Kalirai, J., Niemack, M., Ozel, F., Reynolds, C., Roberge, A., Straughn, K. S. A., Weinberg, D., and Zmuidzinas, J., "Enduring Quests-Daring Visions (NASA Astrophysics in the Next Three Decades)," *ArXiv e-prints* (Jan. 2014).